scientific reports

Check for updates

OPEN

Biocompatibility and antioxidant effects of hydroxyapatite-quercetin composites: in vitro and in ovo studies

Damian Bień[1]✉, Agata Lange[2], Arkadiusz Matuszewski[3], Agnieszka Ostrowska[2], Martyna Klimek[4], Martyna Batorska[1] & Sławomir Jaworski[2]

Hydroxyapatite (HaP) is a biomaterial valued for its biocompatibility and osteoconductive properties, making it suitable for implantology and tissue engineering. The natural flavonoid quercetin (Q) exhibits potent antioxidant and anti-inflammatory effects that support wound healing and reduce oxidative stress. This study assessed the combined impact of HaP and Q on fibroblast viability, oxidative stress markers, and cell migration. The in ovo model evaluated systemic effects via morphometric parameters and oxidative stress in embryonic liver tissue.

Results show that Q significantly decreased oxidative stress by increasing antioxidant enzyme activity and reducing intracellular ROS levels in fibroblasts and embryonic liver ($p < 0.05$). HaP alone induced a mild pro-oxidant response, but its combination with Q (QHaP) led to a marked reduction in oxidative stress markers, indicating a protective synergistic effect. Scratch assay revealed that Q and QHaP enhanced fibroblast migration at all concentrations, with HaP_{10} showing the highest wound closure (93.8%) and $QHaP_{10}$ reaching 89.9% ($p < 0.05$). The in ovo model confirmed that QHaP-treated embryos developed normally, while Q improved embryonic antioxidant defenses. These findings suggest that QHaP composites are promising biocompatible materials that reduce oxidative stress and promote fibroblast migration for wound healing and tissue regeneration.

Keywords Hydroxyapatite, Quercetin, Oxidative stress, Fibroblast, Chicken embryo, Composite

Biomedicine, tissue engineering, and pharmacology increasingly employ nanotechnology to develop innovative solutions for regenerative therapy and oxidative stress-related disorders. Among such materials, hydroxyapatite (HaP) is widely studied due to its excellent biocompatibility and osteoconductive properties, making it suitable for implantology, orthopedics, and dentistry[1]. HaP promotes bone cell adhesion and proliferation, which supports its use in bone grafts and implant coatings[2–5]. As a scaffold component, HaP is often combined with polymers to regulate pore size, cell proliferation, and tissue integration[4,6]. Its properties can be enhanced by the addition of titanium dioxide (TiO_2), which improves antimicrobial activity and may reduce inflammation-related oxidative stress[7].

Conventional biomaterials used in wound healing and tissue regeneration include natural polymers such as collagen, alginate, chitosan, hyaluronic acid, and fibrin, which mimic the extracellular matrix and support cell adhesion, migration, and matrix deposition[8–10]. Synthetic polymers like PLGA (poly(lactic-co-glycolic acid) offer customizable mechanical properties and degradation rates, while hybrid biomaterials combining natural and synthetic components improve moisture retention, infection control, and drug delivery[8,11,12]. However, several limitations restrict their broader use: some materials may induce prolonged inflammation, elicit toxic responses, or degrade inappropriately, while others are difficult to fabricate consistently or fail to prevent microbial infections[9,11,13,14]. These challenges underscore the need for novel scaffolds with enhanced biocompatibility, structural stability, and redox-regulating capacity—such as HaP-based composites.

[1]Department of Animal Breeding and Nutrition, Institute of Animal Sciences, Warsaw University of Life Sciences, 8 Ciszewskiego St, 02-786 Warsaw, Poland. [2]Department of Nanobiotechnology, Institute of Biology, Warsaw University of Life Sciences, 8 Ciszewskiego St, 02-786 Warsaw, Poland. [3]Department of Animal Environment Biology, Institute of Animal Sciences, Warsaw University of Life Sciences, 8 Ciszewskiego St, 02-786 Warsaw, Poland. [4]Faculty of Animal Breeding, Bioengineering and Conservation, Warsaw University of Life Sciences, 8 Ciszewskiego St, 02-786 Warsaw, Poland. ✉email: damian_bien@sggw.edu.pl

Although HaP is traditionally applied in bone-related fields, recent studies have extended its evaluation to soft tissues. Its interaction with fibroblasts—critical players in wound healing and tissue repair—is under growing scrutiny. Evidence suggests that HaP nanoparticles (HaP NPs) can induce oxidative stress by elevating reactive oxygen species (ROS) levels and decreasing antioxidant capacity in various cell types, including human blood cells and rat gastric tissues[15–17]. These findings point to the need for further investigation into the oxidative effects of HaP, especially in non-bone cellular environments[7,18].

Quercetin (Q), a bioactive flavonoid widely present in plant-derived foods, exhibits strong antioxidant, anti-inflammatory, and anticancer properties. It modulates ROS levels and regulates antioxidant enzymes, thereby protecting cells from oxidative damage[19]. Q also contributes to wound healing by enhancing fibroblast proliferation, angiogenesis, and collagen deposition, and by promoting inflammatory cell infiltration at injury sites[20]. Its ability to protect skin cells from UV-induced damage and reduce oxidative stress has been confirmed in several studies[21], and Q-based hydrogels have shown efficacy in supporting muscle regeneration through macrophage modulation and oxidative stress attenuation[22].

Oxidative stress, caused by excessive ROS production, plays a key role in cellular damage and impaired tissue regeneration[23,24]. Studies have shown that HaP NPs can suppress the activity of key antioxidant enzymes such as glutathione peroxidase (GSH-Px), superoxide dismutase (SOD), and catalase (CAT), while increasing lipid peroxidation and nitric oxide generation[16,17]. In contrast, Q has been shown to protect against oxidative stress by lowering intracellular ROS and preserving antioxidant enzyme activity[25,26]. Combining Q with HaP may thus enhance the antioxidant profile and biocompatibility of HaP-based materials.

Fibroblast migration, proliferation, and extracellular matrix remodeling are essential for wound healing. The scratch assay is a widely used in vitro model to evaluate fibroblast migration. Both HaP and Q have been shown to influence fibroblast activity and modulate key cellular signaling pathways involved in wound repair[27]. HaP-containing composite membranes enhance fibroblast proliferation and migration, supporting their use in regenerative applications[28,29]. Likewise, Q accelerates wound closure in scratch assays and improves healing outcomes in both in vitro and in vivo models by stimulating fibroblast migration[30,31].

Therefore, this study aimed to evaluate the biocompatibility and redox-modulating effects of a novel composite material consisting of HaP and Q, using both in vitro (human fibroblast culture) and in ovo (*Gallus gallus*) models. We hypothesized that the combination of HaP and Q would exert synergistic effects, reducing intracellular oxidative stress, enhancing antioxidant enzyme activity, and stimulating fibroblast migration more effectively than either compound alone. Furthermore, we assumed that this composite would not negatively affect embryonic development, confirming its biocompatibility and potential applicability in tissue engineering. To test this hypothesis, the study assessed redox balance, antioxidant enzyme activity, ROS levels, cell viability, and wound closure capacity in vitro, as well as embryotoxicity and liver oxidative stress markers in the in ovo model.

Results

Physicochemical analysis of hap, Q, and their complexes

HaP, Q, and their complexes QHaP were characterized at concentrations of 10 ppm and 100 ppm (Fig. 1). At 10 ppm, the Z-average particle size of HaP was 1455 nm, with a low polydispersity index (PdI) of 0.153, indicating moderate size uniformity and minimal aggregation. However, at 100 ppm, the Z-average particle size increased to 1700 nm, with a higher PdI of 0.367, suggesting greater aggregation due to increased particle interactions and reduced electrostatic stabilization. Q showed distinct behavior compared to HaP. At 10 ppm, the Z-average particle size of Q was below 500 nm, with a very low PdI, reflecting excellent dispersibility and size uniformity. This stability persisted at 100 ppm, as no significant increase in particle size or aggregation was observed, highlighting the stable molecular properties of Q in solution. For the QHaP complexes, particle size and aggregation behavior were influenced by both the concentration of HaP and its interaction with Q. At 10 ppm, the Z-average particle size of QHaP complexes ranged from 1335 to 1455 nm, representing a dominant particle population (96.8–100% intensity) with minimal secondary aggregation (~ 1.7% contribution). The PdI at this concentration was low, indicating good stability of the complexes. At 100 ppm, the Z-average particle size increased to 1.584–1700 nm, with secondary aggregates (~ 5499 nm) contributing up to 3.2% of the particle intensity. The PdI also increased slightly, reflecting reduced stability at higher concentrations.

In vitro experiment

Enzymatic antioxidant activity

The CON group displayed the highest catalase (CAT) activity at 0.427 µmoles/min/mL, but all experimental groups demonstrated a significant decrease ($P < 0.001$). The $QHaP_{100}$-treated group displayed the lowest CAT activity at 0.201 µmoles/min/mL. The HaP_{10} and HaP_{100} groups demonstrated the highest glutathione peroxidase (GSH-Px) activity at 27.35 U and 33.35 U, respectively ($P < 0.001$). The $QHaP_{10}$-treated cells showed the lowest GSH-Px activity at 9.49 U. Superoxide dismutase (SOD) activity levels remained constant between groups ($P = 0.323$), with inhibition rates between 28.7% and 34.4% (Fig. 2A-C).

Total antioxidant capacity

The Trolox equivalent antioxidant capacity (TEAC) value reached its highest point in the CON group at 0.412 µM, but Q_{100}-treated cells showed a substantial decrease to 0.151 µM ($P < 0.001$). The TEAC values of all experimental groups except the CON group matched the values of the control group. The Q_{100} and $QHaP_{100}$ groups showed decreased 2,2-diphenyl-1-picrylhydrazyl (DPPH) scavenging activity at 68.6% and 70.1% of the CON group levels, respectively ($P < 0.001$), but other treatments did not produce statistically significant changes (Fig. 2D, E).

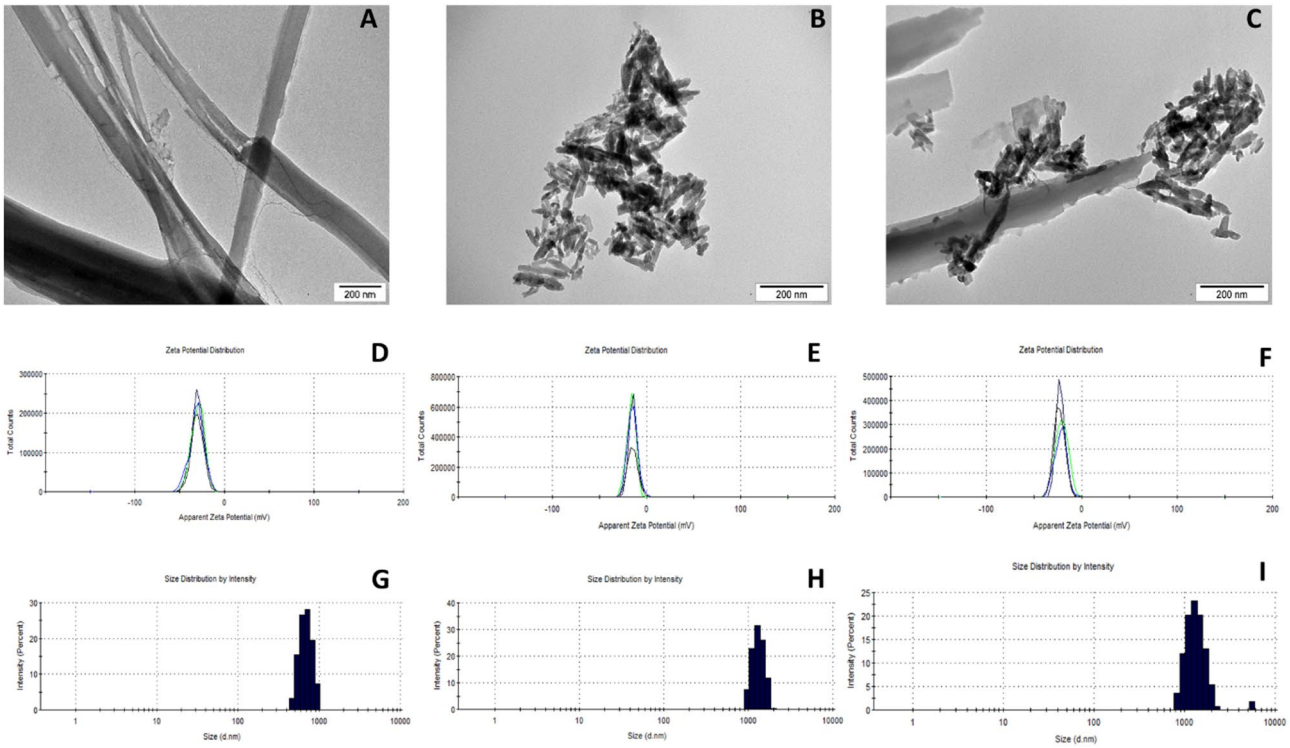

Fig. 1. Physicochemical analysis of Q, HaP, and QHaP (100 ppm). Visualization of materials used by transmission electron microscopy (TEM): **A** Q, **B** HaP, **C** QHaP. Zeta potential graph: **D** Q, **E** HaP, **F** QHaP. Size distribution: **G** Q, **H** HaP, **I** QHaP.

Cell viability and metabolic activity

The Cell Proliferation Kit II (XTT) assay showed the highest metabolic activity in fibroblasts treated with Q_{100} (144.4% of CON; $P < 0.001$). Other treatment groups displayed metabolic activity levels comparable to the CON. The neutral red assay showed the highest membrane integrity in the $QHaP_{100}$-treated group (153.8% of CON; $P < 0.001$), while other experimental groups showed a gradual increase in membrane stability compared to the CON (Fig. 3A, B).

Intracellular ROS levels

Intracellular ROS levels decreased substantially in fibroblasts treated with Q_{100} and Q_{10} after 30 min of incubation, reaching 59.2% of CON and 79.1% of CON, respectively ($P < 0.001$), thus demonstrating strong antioxidant properties of Q. The ROS levels after 40 min showed the lowest values in the Q_{100} (37.8% of CON) and $QHaP_{100}$ (39.3% of CON) groups ($P < 0.001$), indicating a sustained antioxidative effect. The ROS levels in other experimental groups remained variable, without significant changes from the CON. The results show that high concentrations (100 ppm) of Q effectively decrease intracellular ROS levels but simultaneously reduce total antioxidant capacity (TEAC, DPPH). The 100-ppm HaP concentration increased glutathione peroxidase activity and improved membrane integrity, which protects HFFF2 fibroblasts. The $QHaP_{100}$ composite showed a synergistic effect, reducing oxidative stress while improving fibroblast viability, which makes it a promising biocompatible antioxidant agent (Fig. 3C, D).

Scratch assay

The scratch assay demonstrated significant statistical differences in fibroblast migration between the treatment groups (Fig. 4). The HaP_{10} and HaP_{100} groups achieved the highest wound closure percentages at 93.8% and 90.9% respectively, indicating that HaP stimulates cell motility. The values exceeded those for the control group at 72.7% ($P < 0.05$). The Q_{10} group showed moderate migration (84.4%), but Q_{100}-treated cells showed only a small improvement above the control at 77.1%. The $QHaP_{100}$ group demonstrated the lowest wound closure at 76.1%, indicating that high-dose composite does not support fibroblast migration. $QHaP_{10}$-treated cells displayed strong migratory capacity at 89.9%, which matched the results of both HaP groups. The results show that HaP promotes fibroblast migration, and the combination of Q and HaP at low doses produces a synergistic effect. The HaP_{10}, HaP_{100}, and QHaP10 groups showed significant differences from the control group ($P < 0.05$), but Q_{100} and $QHaP_{100}$ did not.

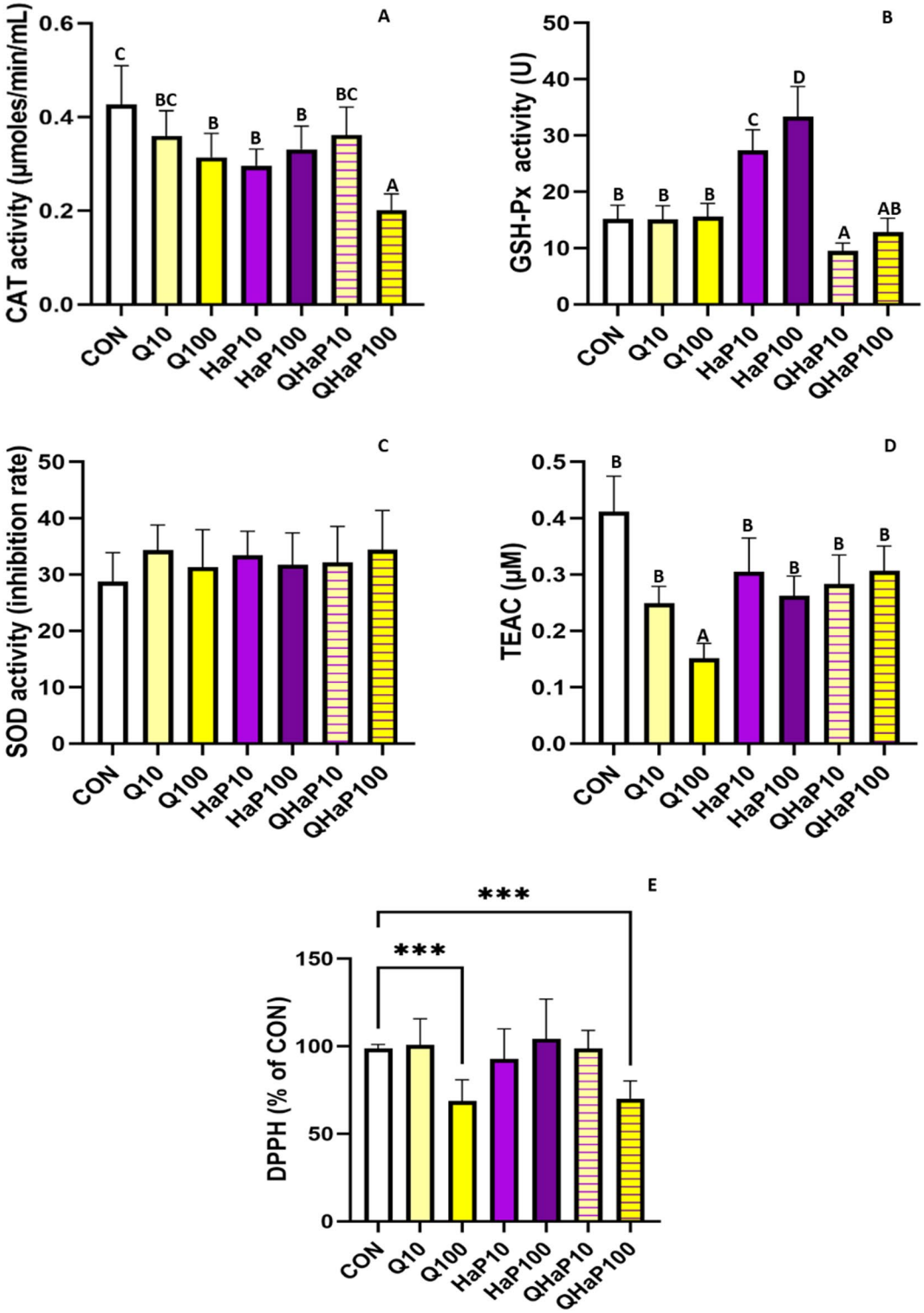

Fig. 2. Antioxidant activity and related parameters in HFFF2 fibroblasts after treatment with quercetin (Q_{10}, Q_{100}), hydroxyapatite (HaP_{10}, HaP_{100}), and their composite ($QHaP_{10}$, $QHaP_{100}$). **A** Catalase (CAT) activity, **B** glutathione peroxidase (GSH-Px) activity, **C** superoxide dismutase (SOD) activity (inhibition rate), **D** Trolox equivalent antioxidant capacity (TEAC), and **E** DPPH scavenging activity expressed as a percentage of the control group (CON). Data are presented as mean ± SD. Significant differences between groups are indicated by different superscript letters ($P < 0.001$). Significant differences between groups are indicated by asterisks (*$P < 0.05$; **$P < 0.01$; ***$P < 0.001$).

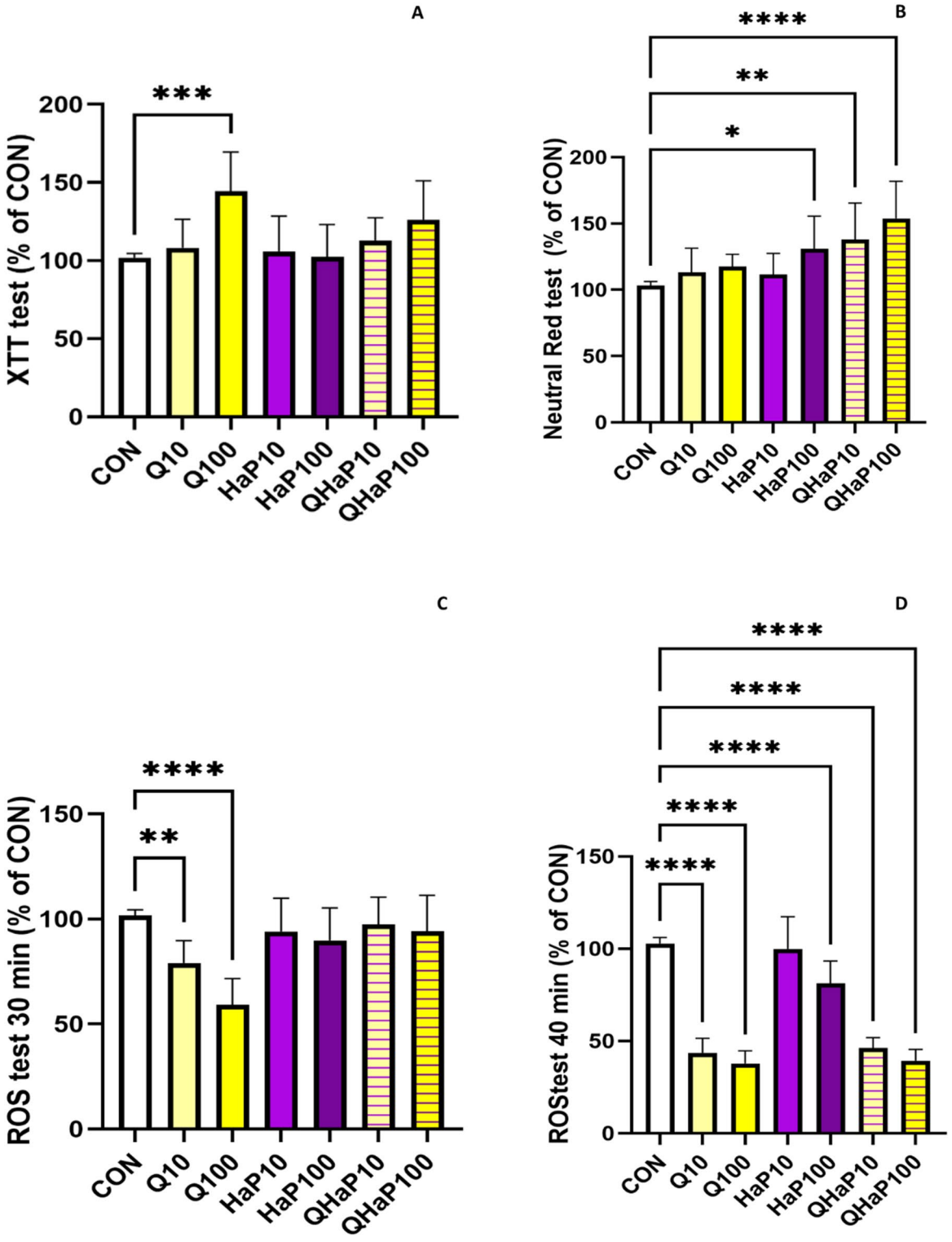

Fig. 3. Cell viability, membrane integrity, and intracellular ROS levels in HFF2 fibroblasts after treatment with quercetin (Q_{10}, Q_{100}), hydroxyapatite (HaP_{10}, HaP_{100}), and their composites ($QHaP_{10}$, $QHaP_{100}$). **A** XTT assay for metabolic activity, **B** neutral red assay for membrane integrity, **C** ROS levels measured after 30 min, and **D** ROS levels measured after 40 min, expressed as a percentage of the control group (CON). Data are presented as mean ± SD. Significant differences between groups are indicated by asterisks (*$P < 0.05$; **$P < 0.01$; ***$P < 0.001$).

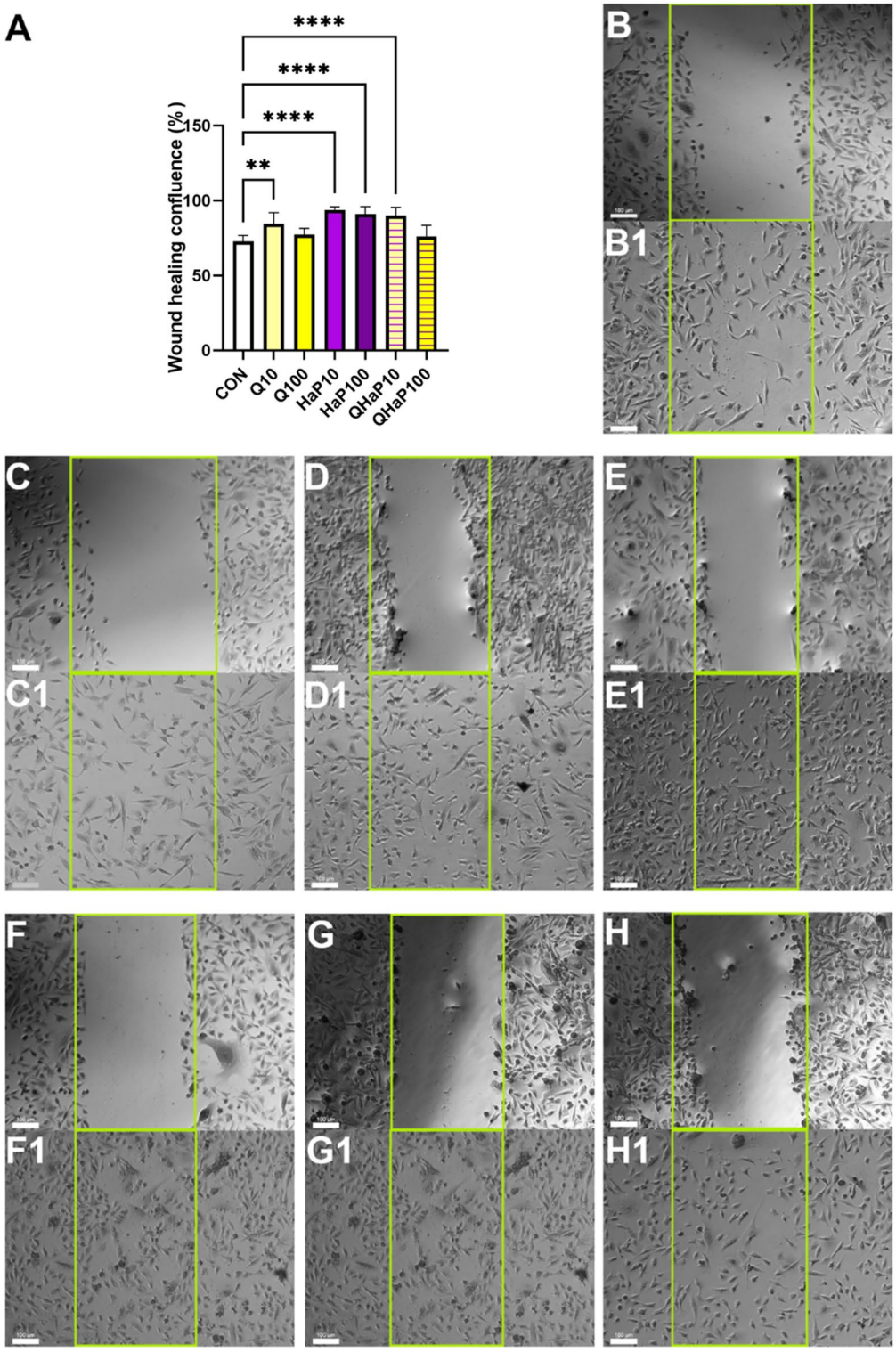

Fig. 4. Wound healing of HFFF2 cell line after exposure to Q, HaP, and QHaP complexes. **A** shows percentage of wound healing confluence in each group related to time 0 h; CON: Control group; Q_{10}: Quercetin 10 ppm; Q_{100}: Quercetin 100 ppm; HaP_{10}: Hydroxyapatite 10 ppm; HaP_{100}: Hydroxyapatite 100 ppm; $QHaP_{10}$: Composite (quercetin + hydroxyapatite) 10 ppm; $QHaP_{100}$: Composite (quercetin + hydroxyapatite) 100 ppm; Values are presented as mean ± SD '*' marks statistically significant differences. **B**–**H1** are exemplary images of wound healing at time 0 h (start of the experiment): **B**–**H**, and at time 24 h: **B1**, **C1**, **D1**, **E1**, **F1**, **G1**, **H1**. **B**, **B1**—control group, **C**, **C1**—Q_{10}, **D**, **D1**—Q_{100}, **E**, **E1**—HaP10, **F**, **F1**—HaP_{100}, **G**, **G1**—$QHaP_{10}$, **H**, **H1**—$QHaP_{100}$. Scale bar = 100 µm. Data are expressed as mean ± SD. Significant differences between groups are indicated by asterisks (*$P < 0.05$; **$P < 0.01$; ***$P < 0.001$).

In ovo experiment

Enzymatic antioxidant activity

The Q_{100}-treated group displayed the lowest catalase (CAT) activity at 1.56 µmoles/min/mL, compared to the CON group with 2.03 µmoles/min/mL ($P<0.001$). The highest CAT activity levels appeared in the $QHaP_{10}$ (2.49 µmoles/min/mL) and HaP_{100} (2.31 µmoles/min/mL) groups, indicating that HaP and its Q composite provide protective effects. The groups treated with HaP displayed elevated glutathione peroxidase (GSH-Px) activity at levels of HaP_{10} (20.24 U), HaP_{100} (21.89 U), $QHaP_{10}$ (24.24 U), and $QHaP_{100}$ (21.74 U), compared to the CON group at 13.46 U ($P<0.001$). The activity of GSH-Px increased significantly in HaP-treated groups because this enzyme plays a vital role in reducing oxidative stress. The SOD activity levels in the CON and Q-treated groups remained constant at 90–95% inhibition, but the HaP_{100}, $QHaP_{10}$, and $QHaP_{100}$ groups showed substantial increases of 118.0%, 107.0%, and 138.0%, respectively ($P<0.001$). The $QHaP_{100}$ group displayed the highest SOD activity, which indicates that Q and HaP may work together to improve superoxide radical scavenging capacity (Fig. 5A).

The study shows that HaP either alone or with Q enhances embryonic liver tissue antioxidant enzyme activities of GSH-Px and SOD and maintains catalase function. Total antioxidant capacity (TEAC) decreases when Q reaches high concentrations (100 ppm), but DPPH scavenging activity increases at lower concentrations. The $QHaP_{100}$ composite displayed the highest SOD activity yet the lowest DPPH scavenging potential, which suggests that enzymatic and non-enzymatic antioxidant systems interact compensatorily (Fig. 5B, C).

Free radical scavenging activity (DPPH assay)

DPPH scavenging activity varied among groups, with the highest values in the Q_{10}-treated group (113.0% of CON) and the lowest in the $QHaP_{100}$ group (77.2% of CON; $P<0.001$). The HaP_{100} group also showed a reduction in DPPH activity (81.7% of CON), potentially indicating an influence of HaP on free radical interactions (Fig. 5D).

Total antioxidant capacity

TEAC levels were significantly lower in the experimental groups (HaP_{10}: 0,333 µM, Hap_{100}: 0,353 µM, Q_{10}: 0.310 µM, Q_{100}: 0.283 µM, $QHaP_{10}$: 0,285 µM, and $QHaP_{100}$: 0,351 µM) compared to the CON group (0.526 µM; $P<0.001$) (Fig. 5E).

Embryo mortality and egg weight

Embryo mortality ranged from 6.67% (HaP_{10}) to 13.34% (CON, Q_{100}, HaP_{100}). The average egg weight varied between 51.16 g (CON) and 59.05 g (Q_{100}), with no significant differences observed among groups ($P=0.606$) (Table 1).

Embryo growth parameters

Embryo body weight did not significantly differ among experimental groups, with values ranging from 20.44 g (HaP_{10}) to 23.22 g ($QHaP_{10}$) ($P=0.398$). Similarly, the embryo-to-egg ratio remained consistent across groups ($P=0.721$), indicating that the tested compounds did not affect overall embryonic growth (Table 1).

Relative organ weights

Liver weight expressed as a percentage of embryo weight showed a significant decrease in the HaP_{10} group at 1.28%, compared to the CON group (2.04%) and other groups ($P<0.001$), which indicates that HaP might affect liver development. Heart weight expressed as a percentage of embryo weight showed a significant increase in the HaP_{10} group at 1.48% compared to the CON group (0.89%) and other groups ($P<0.001$). The observed increase in heart weight could be an adaptive physiological response to HaP exposure. Spleen weight expressed as a percentage of embryo weight showed significant increases in the Q_{10}, Q_{100}, HaP_{100}, and $QHaP_{100}$ groups ($P<0.001$), with the highest value of 0.13% recorded in Q_{100}-treated embryos. The results indicate that in ovo administration of HaP significantly affects liver and heart development, while Q influences spleen size. However, no significant changes were observed in embryo weight or overall growth parameters. These findings suggest that the tested compounds may have organ-specific effects during embryonic development (Table 1).

Discussion

The results show that both HaP and Q have a marked effect on redox status and cell physiology, and that their combination may be synergistic, especially in the context of biomaterials in tissue engineering. The present study demonstrated that the application of Q and HaP, particularly in the form of their complexes (QHaP), significantly influenced redox parameters in the HFFF2 fibroblast model and the development of chicken embryos in ovo.

In the cellular model, HaP at a concentration of 100 ppm significantly increased glutathione peroxidase (GSH-Px) activity, indicating oxidative stress induction and the triggering of compensatory antioxidant pathways. Similar effects were described by Turkez et al.[15], who reported an increase in ROS and antioxidant enzyme activity in response to HaP exposure in cells. In vivo studies also suggest that HaP NPs exposure can transiently reduce GSH levels and enhance lipid peroxidation, subsiding within three weeks as part of a physiological adaptation[32,33]. Concurrently, CAT activity declined in all fibroblast groups, with the lowest level in $QHaP_{100}$, potentially reflecting enzyme-specific inhibition by the QHaP complex[34]. Although SOD activity increased in $QHaP_{100}$, the change was not statistically significant, potentially suggesting modest additional antioxidant pathway activation from the synergistic action of both components.

Quercetin is well recognized for its potent antioxidant effects, with numerous studies reporting a marked reduction in ROS levels due to its free radical-scavenging capacity[23,35,36]. However, the antioxidant effect is dose-dependent—higher concentrations may shift Q's activity towards pro-oxidation. In this study, that effect was

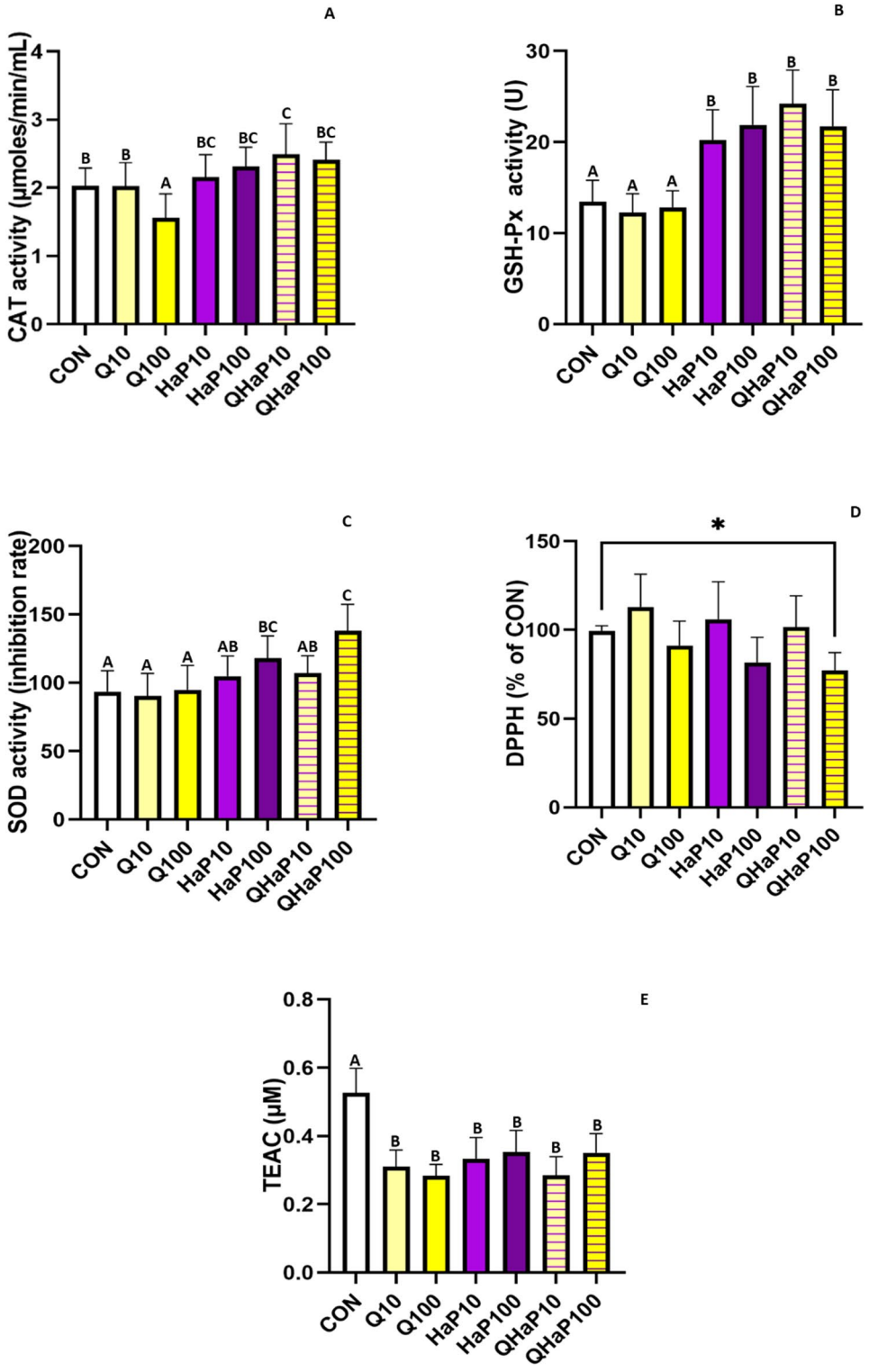

Fig. 5. Antioxidant enzyme activity and free radical scavenging potential in liver tissues of 18-day-old chicken embryos following in ovo administration of quercetin (Q_{10}, Q_{100}), hydroxyapatite (HaP_{10}, HaP_{100}), and their composites ($QHaP_{10}$, $QHaP_{100}$). **A** Catalase (CAT) activity, **B** glutathione peroxidase (GSH-Px) activity, **C** superoxide dismutase (SOD) activity (inhibition rate), **D** DPPH and **E** total antioxidant capacity (TEAC). Data are presented as mean ± SD. Different superscript letters indicate statistically significant differences between groups ($P < 0.001$). Significant differences between groups are indicated by asterisks (*$P < 0.05$).

Parameter	Group							*P* value
	CON	Q_{10}	Q_{100}	HaP_{10}	HaP_{100}	$QHaP_{10}$	$QHaP_{100}$	
Mortality (%)	13.34	10.00	13.34	6.67	10.00	13.34	10.00	–
Egg weight (g)	51.16 ± 8.85	55.68 ± 10.12	59.05 ± 11.10	54.64 ± 11.99	58.61 ± 7.15	54.99 ± 7.89	54.55 ± 10.08	0.606
Embryo weight (g)	20.79 ± 2.91	22.32 ± 3.69	20.64 ± 2.20	20.44 ± 3.14	21.41 ± 2.10	23.22 ± 3.19	20.86 ± 4.28	0.398
Embryo-to-egg ratio (%)	41.73 ± 9.93	40.85 ± 8.06	36.48 ± 9.55	39.40 ± 12.36	36.99 ± 5.82	42.85 ± 7.37	39.70 ± 11.70	0.721
Liver (% of embryo weight)	2.04 ± 0.28^{B}	1.89 ± 0.33^{B}	1.84 ± 0.27^{B}	1.28 ± 0.39^{A}	2.03 ± 0.31^{B}	1.71 ± 0.28^{B}	1.92 ± 0.25^{B}	< 0.001
Heart (% of embryo weight)	0.89 ± 0.16^{A}	0.86 ± 0.15^{A}	0.88 ± 0.15^{A}	1.48 ± 0.32^{B}	0.92 ± 0.14^{B}	0.87 ± 0.11^{B}	1.11 ± 0.21^{B}	< 0.001
Spleen (% of embryo weight)	0.06 ± 0.01^{A}	0.11 ± 0.02^{B}	0.13 ± 0.02^{B}	0.08 ± 0.01^{A}	0.11 ± 0.01^{B}	0.08 ± 0.01^{A}	0.10 ± 0.02^{B}	< 0.001

Table 1. Morphometric parameters of 18-day-old chicken embryos following in Ovo administration of Quercetin (Q_{10}, Q_{100}), hydroxyapatite (HaP_{10}, HaP_{100}), and their composites ($QHaP_{10}$, $QHaP_{100}$). CON: Control group; Q_{10}: Quercetin 10 ppm; Q_{100}: Quercetin 100 ppm; HaP_{10}: Hydroxyapatite 10 ppm; HaP_{100}: Hydroxyapatite 100 ppm; $QHaP_{10}$: Composite (quercetin + hydroxyapatite) 10 ppm; $QHaP_{100}$: Composite (quercetin + hydroxyapatite) 100 ppm; Values are presented as mean ± SD. Different superscript letters within a row indicate statistically significant differences between groups ($P < 0.01$).

reflected in reduced TEAC in fibroblasts and embryonic liver, confirming earlier reports of enhanced ROS and cytotoxicity at higher Q doses[36–39]. This pro-oxidant behavior is associated with Q auto-oxidation and GSH depletion, aligning with observed enzymatic activity reductions in Q_{100}.

Among the tested variants, the $QHaP_{100}$ complex emerged as the most effective, providing superior antioxidant protection and cell membrane stability. Concurrently, GSH-Px and SOD activities were elevated, supporting the literature that links HaP functionalization with Q to enhanced bioactivity and tissue repair capacity[40,41]. The findings from this study strengthen the evidence for a synergistic interaction between HaP and Q when used as a composite (QHaP). Compared to individual agents, QHaP significantly lowered intracellular ROS levels and enhanced antioxidant enzyme activity in fibroblasts. In addition, QHaP promoted fibroblast migration in the scratch assay, indicating regenerative support. This synergistic effect likely results from Q acting as a potent free radical scavenger, while HaP provides a bioactive scaffold that modulates cell function. Though the molecular basis of this synergy remains to be elucidated, the composite consistently outperformed its individual components. Follow-up studies are needed to confirm whether this interaction is additive or genuinely synergistic at the molecular level.

The wound-healing potential of flavonoids, including Q, is well documented. Experimental, animal, and clinical studies have explored Q as an adjuvant agent[42]. Our findings support these observations, showing that wound closure with 10 ppm Q surpassed the control group[30]. Kartal et al.[43] observed enhanced surface closure at 10 and 20 µM but not at 320 µM, which is comparable to our results. HaP also increased wound closure, possibly through calcium ion release, which promotes skin regeneration[44]. Literature supports the idea that HaP and Q form a regenerative synergy[38], with chitosan similarly supporting cartilage regeneration[45]. In our study, surface closure was significantly greater in $QHaP_{10}$ but not in $QHaP_{100}$, likely due to excessive Q content in the latter. These results underscore the importance of precise dose optimization.

The in ovo tests confirmed the biocompatibility of all tested concentrations of HaP, Q, and QHaP, as no adverse effects on embryo survival or hatch weight were observed. Q_{100} and $QHaP_{100}$ showed lower TEAC values in liver tissue, echoing cellular findings and suggesting oxidative stress at higher flavonoid doses. Yu et al.[46] showed that Q up to 40 nmol/egg could mitigate LPS-induced embryonic damage by lowering oxidative and inflammatory stress. HaP_{100} was associated with reduced liver and elevated heart mass, possibly reflecting adaptation to oxidative stress and nanoparticles. Matuszewski et al.[47] found no embryo weight or hatchability changes after HaP nanoparticle exposure in ovo, although they noted minor metabolic alterations.

Although the scratch assay remains under refinement, evidence shows that both HaP and Q affect fibroblast migration. HaP stimulates connective tissue activity and collagen production, while Q reduces ROS and inflammation, enhancing cell migration[31]. The enhanced redox state and membrane stability in $QHaP_{100}$ support its potential for wound-healing applications. Reports suggest that QHaP forms a regenerative niche through local flavonoid release, minimizing oxidative stress and inflammation at implant sites[41].

The synergistic effects of HaP and Q have been attributed to their combined regulation of oxidative stress and cellular signaling pathways. Q scavenges reactive oxygen species and activates antioxidant defenses through pathways such as Nrf2, MAPK, and NF-κB, while its incorporation into HaP scaffolds further enhances antioxidant enzyme activity, including SOD, CAT, and GSH-Px[48–52]. This combination has been shown to improve cellular responses, leading to increased proliferation, migration, and differentiation of bone marrow stem cells, processes also critical for fibroblast-mediated wound healing[52]. In vivo studies confirm that HaP with Q provides sustained release, enhanced antioxidant activity, and superior bone defect repair compared to single agents[40,51–53]. Collectively, these findings demonstrate that the synergy of HaP and Q results from enhanced antioxidation protection, improved cell migration, and regulated remodeling processes, which may explain the beneficial effects observed in our fibroblast model. The present results align with existing data indicating the benefits of HaP and Q, particularly when used in combination. The QHaP complex offered greater protection than either component alone, minimizing oxidative stress while promoting fibroblast survival. These findings support the use of QHaP for implant coatings or bioactive scaffolds in tissue regeneration. Recent data reinforce

the role of QHaP in regenerative medicine, particularly in skin, bone, and soft tissue applications. HaP is reported to have minimal genotoxic potential, and in some cases, may protect host DNA[32].

The QHaP composite exhibits synergistic effects by reducing reactive oxygen species (ROS), enhancing antioxidant enzyme activity, and supporting cellular function and tissue development. These outcomes suggest its potential use in regenerative medicine, particularly as a bioactive scaffold or implant coating. However, several limitations of the present study should be considered. The results were obtained using in vitro and in ovo models, which, despite their value, do not fully replicate the biological complexity of mammalian systems. While the chicken embryo model provides insights into developmental biocompatibility, its direct clinical applicability remains limited. Consequently, long-term in vivo studies in mammalian models are required to assess wound healing, immune responses, and tissue integration, as well as to validate the safety and therapeutic efficacy of QHaP composites. Moreover, the molecular mechanisms underlying the observed synergy between HaP and Q remain insufficiently understood. Further investigations should focus on identifying specific signaling pathways and gene expression profiles responsible for the composite's bioactivity. Particular attention should be paid to the dose-dependent dual role of Q as both an antioxidant and a pro-oxidant, which emphasizes the need for precise formulation and delivery strategies in future applications.

Conclusion

This study demonstrated that HaP and Q, both individually and in combination, modulate redox homeostasis and fibroblast functionality in a dose-dependent manner. The QHaP composite exerted synergistic effects, especially at lower concentrations, enhancing antioxidant defense and supporting cell migration while maintaining embryonic biocompatibility. These findings underscore the potential of QHaP as a bioactive scaffold component or coating material in regenerative medicine. Future research should focus on the molecular mechanisms underlying this synergy and the validation of efficacy in mammalian in vivo models.

Methods

Quercetin (Q)

Quercetin (≥95% purity, HPLC grade) was obtained from Sigma-Aldrich (product number: Q4951, CAS: 117-39-5) in the form of powder. The compound is a natural flavonoid with antioxidant properties, and this study evaluated its impact on antioxidant activity and particle stability in QHaP complexes. Before it was used in experiments, a stock solution was prepared by weighing 0.05 g and adding 50 mL of sterile ultrapure water. For use in experiments, the stock solution was diluted to the appropriate concentration.

Hydroxyapatite (HaP)

HaP NPs (HaP, ≥97% purity, nanometer-sized powder, CAS: 1306-06-5) were obtained from SkySpring Nanomaterials, Inc., in the form of powder. The material, with a chemical composition of $Ca_{10}(PO_4)_6(OH)_2$, was characterized by a high surface area and nanoscale dimensions, making it suitable for applications in biomaterials research. Before it was used in experiments, a stock solution was prepared by weighing 0.05 g and adding 50 mL of sterile ultrapure water. For use in experiments, the stock solution was diluted to the appropriate concentration.

Complexes (QHaP)

Complexes were prepared by mixing two components in appropriate proportions, followed by sonication (500 W, 30 kHz, 2 min) using a Vibra-Cell™ Ultrasonic Liquid Processor (Sonics & Materials, Newton, CT, USA). The sonicated complexes were left at room temperature for 15 min to combine the components (forced self-assembly).

Experimental design

Physicochemical analysis

HaP, Q, and their complexes (QHaP) were analyzed by measuring the hydrodynamic diameter by dynamic light scattering (DLS) and measuring the zeta potential by electronic light scattering (ELS) with the use of Zetasizer Nano-ZS ZEN 3600 (Malvern Instruments Ltd., Malvern, UK). All measurements were conducted at room temperature (23 °C), at least three times. Additionally, the materials used were visualized by transmission electron microscopy (TEM) using a microscope (TEM, JEM-1220, JEOL, Tokyo, Japan) operated at a voltage of 80 keV, by placing the solutions on a copper grid (3 mm 200 mesh Cu grids, Formvar, Agar Scientific, Stansted, UK). Samples were dried and observed immediately.

Cell culture and cytotoxicity assessment

Human fibroblasts (*Homo sapiens*), HFFF2 cell line derived from fetal foreskin, were used in this study. The HFFF2 cell line was obtained from the American Type Culture Collection (ATCC, Manassas, VA, USA). The cells were normal, adherent fibroblasts, stored in a frozen state in the vapor phase of liquid nitrogen until use. The cultures were maintained in DMEM Low Glucose medium (Biowest, Nuaillé, France) supplemented with 10% fetal bovine serum (Gibco, Grand Island, NY, USA) and 1% penicillin/streptomycin (Gibco, Grand Island, NY, USA). The cells were grown in 96-well plates ($1.5*10^5$ cells/mL) at 37 °C in a humidified atmosphere of 95% air and 5% CO_2. Prepared plates were then exposed to Q, HaP, and QHaP (final concentration 10 or 100 ppm for each factor) for 24 h. After incubation, cell viability and cytotoxicity were assessed using the Cell Proliferation Kit II (XTT) (Roche, Basel, Switzerland). XTT reagent was added to each well (30 µL/well), and the plate was incubated for an additional 4 h under the same conditions. Absorbance was then measured using a spectrophotometer at a wavelength of 450 nm, with a reference wavelength of 690 nm. Each test was performed

in triplicate. This assay allowed for the quantification of metabolic activity, serving as an indicator of cell viability and cytotoxicity. For experimental procedures, fibroblasts were detached from the culture surface using trypsin (Gibco, Grand Island, NY, USA) and subsequently collected for further analysis. Results were expressed as a percentage of the mean value of each group in relation to CON.

Chicken embryo

The study material consisted of 210 fertilized chicken eggs sourced from 37-week-old Ross × Ross 308 hens, obtained from a certified commercial hatchery. All eggs were collected on the same day and belonged to a uniform weight class. After collection, the eggs were stored at 12 °C with 73% relative humidity for 2 days before being transferred to an incubator (Jamesway, Canada).

On the first day of incubation, the eggs were weighed and randomly assigned to experimental groups, each consisting of 30 eggs: one control group without injection and six treatment groups: Q_{10}, Q100, HaP10, HaP100, $QHaP_{10}$, and $QHaP_{100}$ at 10 and 100 ppm concentrations. Prior to injection, the eggs were disinfected by immersion in a 0.5% potassium permanganate solution. A volume of 0.2 mL of the respective hydrocolloid was injected into the albumen under sterile conditions using 27-gauge, 20-mm needles. The injection sites was immediately sealed with sterile tape to prevent contamination, and the eggs were returned to the incubator.

The eggs were incubated for a total of 18 days under standard conditions: 37.8 °C and 55% humidity, with automatic turning once per hour. Embryo development was monitored on days 7 and 14 using candling to ensure proper development and identify any embryonic mortality.

Neutral red test

To assess cytotoxicity, the neutral red assay was performed by adding Neutral Red solution (Sigma, Saint Louis, MO, USA) to each well, followed by incubation for 10 min under the same conditions. Absorbance was measured using a spectrophotometer at a wavelength of 540 nm, providing an indicator of cell viability and cytotoxicity. Results were expressed as a percentage of the mean value of each group in relation to the control.

Antioxidant analysis using DPPH assay

To perform the antioxidant analysis, a solution of DPPH (Sigma, Saint Louis, MO, USA) in methanol was prepared and added to a 24-well plate. Q, HaP nanoparticles, and their composite, suspended in ultrapure water, were subsequently added to the wells. The plate was incubated for 10 min in the dark, after which the samples were transferred to a 96-well plate in triplicate for each original well. Absorbance was measured using a spectrophotometer at a wavelength of 515 nm. To assess the inhibition of free radicals (DPPH) in chicken embryonic liver cells, livers were homogenized and placed in a 24-well plate. A DPPH solution in methanol was then added, and the plate was incubated for 10 min in the dark. After incubation, the samples were transferred to a 96-well plate in triplicate for each original well, and absorbance was measured at 515 nm using a spectrophotometer.

Scratch assay

Fibroblasts were seeded into a 24-well plate and treated with Q, HaP NPs, and their composite. A scratch was made in each well to simulate a wound. To stain the initial control well (time 0), May-Grünwald stain (Sigma, Saint Louis, MO, USA) and Giemsa stain (Sigma, Saint Louis, MO, USA) were applied. The plate was then incubated for 24 h at 37 °C in a humidified atmosphere of 95% air and 5% CO_2. After the incubation period, the remaining wells were stained using the same method as that used for the control well. Images of fibroblasts at the scratch site were captured under a microscope to evaluate wound closure and cell migration. The percent wound healing confluence was calculated as:

$$\frac{(t_0 - t_{24}) \cdot 100\%}{t_0},$$

where t_0 is initial area of scratch wound and t_{24} is area of scratch wound at time 24 h[54]. Measurements were made using the ImageJ program (version 1.50e, USA) with the wound healing size tool plugin.

Ethical statement

The ethics review board II of the Local Committee for Ethics in Animal Research of Warsaw University of Life Sciences—SGGW finds that this type of project does not fall under the legislation for the protection of animals used for scientific purposes, national decree-law (Dz. U. 2015 poz. 266 and 2010–63-EU directive). The study was carried out in compliance with the ARRIVE guidelines 2.0.

Statistical analysis

Statistical analyses were performed using PS IMAGO PRO 10 (IBM SPSS Statistics) and GraphPad Prism 9 (GraphPad Software, San Diego, CA, USA). Data were initially tested for normality using the Shapiro-Wilk test. For comparisons involving more than two groups, one-way analysis of variance (ANOVA) followed by Tukey's post hoc test was used. When individual experimental groups were directly compared to the control group (CON), independent samples t-tests were applied. All data are presented as mean ± standard deviation (SD). Statistical significance was considered $P < 0.05$. Graphs and visualizations were generated in GraphPad Prism 9. Statistically significant differences are indicated by different superscript letters (ANOVA) or asterisks (*$P < 0.05$; **$P < 0.01$; ***$P < 0.001$) for t-tests.

Data availability

The datasets used and/or analyzed during the current study are available from the corresponding author upon reasonable request.

Received: 2 July 2025; Accepted: 22 August 2025
Published online: 27 August 2025

References

1. Dorozhkin, S. V. Bioceramics of calcium orthophosphates. *Biomaterials* **31**, 1465–1485 (2010).
2. Jiang, Y., Yuan, Z. & Huang, J. Substituted hydroxyapatite: a recent development. *Mater. Technol.* **35**, 785–796 (2020).
3. Nabipour, H., Batool, S. & Hu, Y. Chemical surface modification of hydroxyapatite for biomedical application: a review. *Emerg. Mater.* **6**, 31–44 (2023).
4. Stella, S. M. & Vijayalakshmi, U. Influence of polymer based scaffolds with Genipin cross linker for the effective (pore size) usage in biomedical applications. *Trends Biomater. Artif. Organs*. **32**, 83–92 (2018).
5. Fathi, M. H., Mortazavi, V., Hanifi, A. & Roohani, S. I. Synthesis, characterization and bioactivity evaluation of nano-structured hydroxyapatite. *WIT Trans. Eng. Sci.* **64**, 309–317 (2009).
6. Sobczak-Kupiec, A., Tomala, A. M., Domínguez López, C., Drabczyk, A. & Tyliszczak, B. Polymer–ceramic biocomposites based on pvp/histidine/hydroxyapatite for hard tissue engineering applications. *Int. J. Polym. Mater. Polym. Biomater*. **71**, 1380–1392 (2022).
7. Asyiah, E. N., Irwansyah, F. S., Noviyanti, A. R. & Eddy, D. R. Composite of hydroxyapatite (HA) from eggshells and TiO2. in *AIP Conference Proceedings* pp 2646 (American Institute of Physics Inc., 2023).
8. Jalise, S. Z. & Sheykhhasan, M. Role of biomaterials in promoting wound healing. In *Innovations and Applications of Advanced Biomaterials in Healthcare and Engineering* 367–411 (IGI Global, 2025).
9. Prasathkumar, M. & Sadhasivam, S. Chitosan/hyaluronic acid/alginate and an assorted polymers loaded with honey, plant, and marine compounds for progressive wound healing—know-how. *Int. J. Biol. Macromol.* **186**, 656–685 (2021).
10. Gao, Y. et al. Research advances of natural biomaterials in promoting wound repair. *Chin. J. Burns Wounds*. **39**, 481–486 (2023).
11. Aramwit, P. Introduction to biomaterials for wound healing. In *Wound Healing Biomaterials*. 2 pp 3–38 (Elsevier Inc., 2016).
12. Liu, W. et al. Tailored biomedical materials for wound healing. *Burns Trauma* **11**, 1–19 (2023).
13. Lynch, R. I. & Lavelle, E. C. Immuno-modulatory biomaterials as anti-inflammatory therapeutics. *Biochemical Pharmacol.* **197**, 114890 (2022).
14. Alven, S., Mbese, Z., Peter, S., Feketshane, Z. & Aderibigbe, B. A. The efficacy of injectable biomaterials for wound care, orthopedic application, and tissue engineering. *Polym. Biomater. Healthc. Appl.* **2022**, 285–334 (2022).
15. Turkez, H. et al. Evaluation of cytotoxic, oxidative stress and genotoxic responses of hydroxyapatite nanoparticles on human blood cells. *J. Appl. Toxicol.* **34**, 373–379 (2014).
16. Mosa, I. F., Abd, H. H., Abuzreda, A., Assaf, N. & Yousif, A. B. Bio-evaluation of the role of chitosan and curcumin nanoparticles in ameliorating genotoxicity and inflammatory responses in rats' gastric tissue followed hydroxyapatite nanoparticles' oral uptake. *Toxicol. Res.* **9**, 493–508 (2021).
17. Yousef, M. I., Abd, H. H., Helmy, Y. M. & Kamel, M. A. N. Synergistic effect of curcumin and chitosan nanoparticles on nano-hydroxyapatite-induced reproductive toxicity in rats. *Environ. Sci. Pollut. Res.* **28**, 9362–9376 (2021).
18. Kazimierczak, P. et al. Hydroxyapatite or Fluorapatite—Which bioceramic is better as a base for the production of bone Scaffold? A comprehensive comparative study. *Int. J. Mol. Sci.* **24** (6), 5576 (2023).
19. Boots, A. W., Haenen, G. R. M. M. & Bast, A. Health effects of quercetin: from antioxidant to nutraceutical. *Eur. J. Pharmacol.* **585**, 325–337 (2008).
20. Kant, V., Jangir, B. L., Kumar, V., Nigam, A. & Sharma, V. Quercetin accelerated cutaneous wound healing in rats by modulation of different cytokines and growth factors. *Growth Factors*. **38**, 105–119 (2020).
21. Hatahet, T. et al. Quercetin topical application, from conventional dosage forms to nanodosage forms. *Eur. J. Pharm. Biopharm.* **108**, 41–53 (2016).
22. Wang, Y. et al. Quercetin-based composite hydrogel promotes muscle tissue regeneration through macrophage polarization and oxidative stress attenuation. *Compos. Part B Eng.* **247** (218), 110311 (2022).
23. Zhang, Y. M., Zhang, Z. Y. & Wang, R. X. Protective mechanisms of Quercetin against myocardial ischemia reperfusion injury. *Front. Physiol.* **11**, 956 (2020).
24. Khursheed, R., Singh, S. K., Wadhwa, S., Gulati, M. & Awasthi, A. Enhancing the potential preclinical and clinical benefits of Quercetin through novel drug delivery systems. *Drug Discov. Today* **25**, 209–222 (2020).
25. Zhang, N., Zhang, H. X., Ma, X. L. & Hong, J. N. Protective effects of Quercetin against H2O2 induced KGN cells injury. *Tradit. Med. Res.* **9** (2), 7 (2024).
26. Bagheri, A., Ebrahimpour, S., Nourbakhsh, N., Talebi, S. & Esmaeili, A. Protective effect of Quercetin on alteration of antioxidant genes expression and histological changes in the dental pulp of the streptozotocin-diabetic rats. *Arch. Oral Biol.* **125**, 105088 (2021).
27. Pastar, I. et al. Epithelialization in wound healing: a comprehensive review. *Adv. Wound Care*. **3**, 445–464 (2014).
28. Ariesanti, Y., Poedjiastoeti, W., Sriyanto, G. A. & Angraini, Y. Increase of fibroblast proliferation by composite membrane (polyvinyl alcohol-collagen-hydroxyapatite), In *InHeNce 2021–2021 IEEE International Conference on Health, Instrumentation and Measurement, and Natural Sciences* (Institute of Electrical and Electronics Engineers Inc., 2021).
29. Zhang, S. et al. Development of a multifunctional nano-hydroxyapatite platform (nHEA) for advanced treatment of severely infected full-thickness skin wounds. *Acta Biomater.* **181**, 440–452 (2024).
30. Chittasupho, C., Manthaisong, A., Okonogi, S., Tadtong, S. & Samee, W. Effects of Quercetin and Curcumin combination on antibacterial, antioxidant, in vitro wound healing and migration of human dermal fibroblast cells. *Int. J. Mol. Sci.* **23**, 142 (2022).
31. Mi, Y. et al. Quercetin promotes cutaneous wound healing in mice through Wnt/β-catenin signaling pathway. *J. Ethnopharmacol.* **290**, 115066 (2022).
32. de Souza, A. M. et al. Are hydroxyapatite-based biomaterials free of genotoxicity? A systematic review. *Chemosphere* **352**, 141383 (2024).
33. Lekshmy, M. S., Gayathri, V., Sabareeswaran, A. & Mohanan, P. V. Induction of oxidative stress and lymphocyte proliferation by nanohydroxyapatite in mice. *J. Basic Appl. Res. Int.* **8** (3), 202–212 (2015).
34. Pappus, S. A. et al. A toxicity assessment of hydroxyapatite nanoparticles on development and behaviour of drosophila melanogaster. *J. Nanopart. Res.* **19** (4), 1–16 (2017).
35. Tian, R., Yang, Z., Lu, N. & Peng, Y. Y. Quercetin, but not rutin, attenuated hydrogen peroxide-induced cell damage via Heme oxygenase-1 induction in endothelial cells. *Arch. Biochem. Biophys.* **676**, 108157 (2019).
36. Rizvi, S. I. & Mishra, N. Anti-oxidant effect of Quercetin on type 2 diabetic erythrocytes. *J. Food Biochem.* **33**, 404–415 (2009).
37. Metodiewa, D., Jaiswal, A. K., Cenas, N., Dickancaité, E. & Segura-Aguilar, J. Quercetin may act as a cytotoxic prooxidant after its metabolic activation to semiquinone and quinoidal product. *Free Radic. Biol. Med.* **26**, 107–116 (1999).

38. Lee, S. et al. Hydroxyapatite microbeads containing BMP-2 and Quercetin fabricated via electrostatic spraying to encourage bone regeneration. *Biomed. Eng. Online*. **22**, 1–16 (2023).
39. Fonseca-Silva, F., Inacio, J. D. F. & Canto-Cavalheiro, M. M. & Almeida-Amaral, E. E. Reactive oxygen species production and mitochondrial dysfunction contribute to Quercetin induced death in leishmania amazonensis. *PLoS One* **6** (2), 14666 (2011).
40. Forte, L. et al. Antioxidant and bone repair properties of quercetin-functionalized hydroxyapatite: an in vitro osteoblast-osteoclast-endothelial cell co-culture study. *Acta Biomater.* **32**, 298–308 (2016).
41. Furlani, F. et al. Designing bioinspired multifunctional nanoplatforms to support wound healing and skin regeneration: Mg-hydroxyapatite Meets melanins. *Colloids Surf B Biointerfaces*. **235**, 113756 (2024).
42. Zulkefli, N. et al. Flavonoids as potential wound-healing molecules: emphasis on pathways perspective. *Int. J. Mol. Sci.* **24**, 4607 (2023).
43. Kartal, B., Alimogullari, E., Elçi, P., Fatsa, T. & Ören, S. The effects of Quercetin on wound healing in the human umbilical vein endothelial cells. *Cell. Tissue Bank.* **25**, 851–860 (2024).
44. Gao, J. et al. Biopaper based on ultralong hydroxyapatite nanowires and cellulose fibers promotes skin wound healing by inducing angiogenesis. *Coatings* **12**, 479 (2022).
45. Panbhukarasu, S. et al. Integrated network Pharmacology and bio-functional chitosan-hydroxyapatite scaffolds incorporating Quercetin for enhanced bone regeneration in articular cartilage defects. *J. Bioact. Compat. Polym.* **40** (3), 248–266 (2025).
46. Yu, J., Hu, G., Guo, X., Cao, H. & Zhang, C. Quercetin alleviates inflammation and energy deficiency induced by lipopolysaccharide in chicken embryos. *Animals* **13**, 2051 (2023).
47. Matuszewski, A. et al. Effect of in ovo application of hydroxyapatite nanoparticles on chicken embryo development, oxidative status and bone characteristics. *Arch. Anim. Nutr.* **74**, 343–361 (2020).
48. Khan, F. et al. Molecular targets underlying the anticancer effects of quercetin: an update. *Nutrients* **8** (9), 29(2016).
49. Yang, Y. et al. Metal-free antioxidant nanozyme incorporating bioactive hydrogel as an antioxidant scaffold for accelerating bone reconstruction. *Biomaterials* **320**, 123285 (2025).
50. Hong, G. et al. Therapeutic potential of a prominent dihydroxyflavanone pinocembrin for osteolytic bone disease: in vitro and in vivo evidence. *J. Orthop. Transl.* **45**, 197–210 (2024).
51. Tripathi, G., Raja, N. & Yun, H. S. Effect of direct loading of phytoestrogens into the calcium phosphate scaffold on osteoporotic bone tissue regeneration. *J. Mater. Chem. B.* **3**, 8694–8703 (2015).
52. Ren, M. et al. Enhanced bone formation in rat critical-size tibia defect by a novel quercetin-containing alpha-calcium sulphate hemihydrate/nano-hydroxyapatite composite. *Biomed. Pharmacother.* **146**, 112570 (2022).
53. Forte, L. et al. Quercetin and alendronate multi-functionalized materials as tools to hinder oxidative stress damage. *J. Biomed. Mater. Res. Part. A*. **105**, 3293–3303 (2017).
54. Buachan, P., Chularojmontri, L. & Wattanapitayakul, S. K. Selected activities of citrus maxima merr. Fruits on human endothelial cells: enhancing cell migration and delaying cellular aging. *Nutrients* **6**, 1618–1634 (2014).

Acknowledgements
Correspondence and requests for materials should be addressed to D.B.

Author contributions
Conceptualization, D.B., and S.J.; methodology, D.B.; software, M.B.; validation, A.O., M.K., M.B. and A.L.; formal analysis, D.B.; investigation, D.B., S.J., A.M., A.L., A.O., M.K., M.B.; resources, S.J., D.B., A.M.; data curation, D.B., A.L.; writing-original draft preparation, D.B., A.M.; writing—review and editing, D.B., S.J., A.L.; visualization, A.O., A.L., D.B.; supervision, S.J.; project administration, S.J., D.B.; funding acquisition, S.J., D.B. All authors have read and agreed to the published version of the manuscript.

Funding
This research received no external funding.

Declarations

Competing interests
The authors declare no competing interests.

Additional information
Correspondence and requests for materials should be addressed to D.B.

Reprints and permissions information is available at www.nature.com/reprints.

Publisher's note Springer Nature remains neutral with regard to jurisdictional claims in published maps and institutional affiliations.